ANTENNA OPTIMIZATION FOR ALFVEN WAVE HEATING

Satish Puri

IPP-4/228 Juni 1986

MAX-PLANCK-INSTITUT FÜR PLASMAPHYSIK

8046 GARCHING BEI MÜNCHEN

MAX-PLANCK-INSTITUT FÜR PLASMAPHYSIK

GARCHING BEI MÜNCHEN

ANTENNA OPTIMIZATION FOR ALFVEN WAVE HEATING

Satish Puri

IPP-4/228 Juni 1986

Die nachstehende Arbeit wurde im Rahmen des Vertrages zwischen dem Max-Planck-Institut für Plasmaphysik und der Europäischen Atomgemeinschaft über die Zusammenarbeit auf dem Gebiete der Plasmaphysik durchgeführt.

ANTENNA OPTIMIZATION FOR ALFVEN WAVE HEATING

Satish Puri

Max-Planck Institut für Plasmaphysik

EURATOM Association, D-8046 Garching, FRG

ABSTRACT

Antenna optimization studies for radio-frequency coupling to the Alfven waves is carried out using a self-consistent, three-dimensional, fully-analytic, Faraday-shielded, periodic-loop-antenna model. The antenna characteristics (the loading resistance R, the reactance X, the quality factor Q, and the effeciency η_A) are investigated over a wide range of parameters using the ASDEX UPGRADE parameters as reference. With proper care it is possible to obtain an experimentally acceptable loading of $R \sim 1\Omega$ with an attendent $Q \sim 20$ under optimal conditions. The required conditions consist of (i) locating the singular Alfven layer at about two-thirds the plasma radius, and (ii) the adjacent antenna separation along the toroidal direction is of the order of the plasma radius. This implies using a toroidal wave number $n \sim 8$, for the ASDEX UPGRADE case. The extensive results presented here should facilitate the antenna design for Alfven-wave heating in most existing as well as projected machines. By scaling the linear dimensions of the ASDEX UPGRADE it is shown that the Alfven-wave heating continues to be an attractive alternative even for plasmas of thermonuclear dimensions. Due to the changing plasma conditions during the radio-frequency heating phase, dynamic impedance tracking may become necessary. Methods for maintaining an efficient coupling under these conditions through the phase control of a dense-cluster-array antenna, resembling the lower-hybrid grill coupler, is suggested.

1. INTRODUCTION

Of the set of the two low-frequency, cold-plasma magnetohydrodynamic waves, the slow mode possesses a singular character at the Alfven [1] resonance. Using a kinetic treatment Stepanov [2] showed that the slow mode is strongly Landau damped as the electron thermal speed approaches the longitudinal wave velocity. Winterberg [3] recognized the potential of the Alfven waves for the heating of thermonuclear plasmas. The present spurt of interest in these waves was generated by the work of Grossman and Tataronis [4, 5] who found that the fast compressional Alfven wave launched by the antenna situated near the plasma edge tunnels across the evanescent layer and is efficiently assimilated at the singular layer. Hasegawa and Chen [6, 7] showed that in a hot plasma the singular behaviour is replaced by the partial conversion of the fast compressional mode to the slow torsional kinetic mode (kinetic Alfven wave), which is readily absorbed through electron Landau damping. This pioneering work led the way to much subsequent activity [8 – 19].

For instance, among the notable contributions made by the Lausanne group is the recognition of the discrete-Alfven-waves (DAW) as a possible contender for plasma heating. Unlike the continuum-Alfven-wave (CAW) heating involving essentially a local plasma resonance at the Alfven layer, the DAW resonance involves the bulk plasma response and occurs at frequencies below the Alfven continuum. Despite the shared label of ALFVEN WAVE HEATING, the two heating schemes are physically dissimilar with fundamentally different absorption behaviours. The absorption of CAW occurs through the well understood Landau damping mechanism and may be successfully simulated via the singularity occuring at $\epsilon_r = n_z^2$ (with $k_r \to \infty$) in the cold-plasma approximation. On the other hand, there remains some uncertainty regarding the dissipation of DAW. Unlike the case of CAW heating via the torsional kinetic-Alfven-wave, the hot-plasma effects do not contribute a comparable dissipation mechanism for DAW which has a purely compressional character. The compressional mode is very weakly damped by Landau damping with a radial absorption length of several kilometers [13] which would result in an unacceptably high antenna Q. According to Bernstein [16], since the resistive component of the antenna impedance vanishes identically as the fictitiously introduced collision frequency goes to zero, DAWs though contributing to the reactive loading yield no net absorption and are to be avoided. In this paper we circumvent this controversy by assuming that the DAW excitation is obviated through a judicious choice of the operating frequency and antenna parameters.

Another noteworthy contribution in this field is due to Ross, Chen and Mahajan [14], who have conducted a boundary value analysis incorporating both the fast and the kinetic Alfven waves. The wave conversions as well as the absorption processes are automatically accounted for and the energy deposition profile is directly obtained without recourse to artificial simulation through the introduction of collisional damping. The added complexity due to the presence of fast decaying or growing solutions is tackled by employing a Galerkin procedure with cubic spline elements.

Currently, a great deal of effort is being directed towards global wave solutions in toroidal geometries [11, 16, 19]. Toroidicity causes the expected shift in the singular surface along with the excitation of parasitic azimuthal modes.

In this paper we report the results of an extensive systematic search in the parameter space for the antenna optimization studies conducted using a modified version of the three-dimensional, self-consistent loop-antenna treatment of Ref. 21. The modifications consist of the *fully analytic* determination of the self-consistent antenna current without recourse to the iterative procedures for the case of the single-element antenna of Ref. 21. Furthermore, the self-consistent treatment has been extended to the case of the multiple-loop antennas. The requirement of self-consistency can cause a change in the antenna impedance by as much as 20% compared to the case when a uniform antenna current is assumed.

Our model also includes the Faraday shield interposed between the antenna and the plasma . Under experimental conditions, the Faraday shield is necessary to avoid direct coupling of the torsional Alfven wave to the plasma. In the absence of the Faraday shield, the parasitic coupling will give rise to additional but undesirable antenna loading resulting in surface heating, impurity release and antenna breakdown problems.

Although the antenna coupling is studied in the flat geometry, the plasma surface impedance $\varsigma_f = -E_\phi/H_z$ is obtained in the cylindrical geometry, because the cylindrical effects may become significant in the plasma interior.

The antenna characteristics are computed for a wide range of parameters, spanning those of the existing as well as the projected machines, taking the ASDEX UPGRADE parameters as the reference values. The normalizations and the antenna terminology of Ref. 21 is retained.

Due to the relatively high values of Q encountered during the Alfven wave heating, the antenna input impedance is likely to be sensitive to variations in the plasma parameters. Experimental methods of maintaining a dynamic match between the plasma and the antenna are discussed.

2. PLASMA SURFACE IMPEDANCE

The essential processes involved consist of launching the compressional Alfven wave at the plasma edge, tunneling through the evanescent region, and conversion to the singular mode at the Alfven resonance layer. In a hot plasma, the energy absorption in the resonance region occurs via electron Landau damping [6, 7]. Coupling to the fast wave at the plasma edge is not substantially affected by the thermal effects and a cold-plasma description suffices.

From the Maxwell's equations in the cylindrical geometry, one may obtain the following differential equations for the fast compressional wave upon neglecting terms containing E_z and E_z' (prime denotes differentiation with respect to radius r)

$$E_\phi' = -\frac{1}{r}\,(1 + \frac{m\epsilon_y}{\gamma_1})\,E_\phi + i\,(1 - \frac{m^2}{r^2\gamma_1})\,H_z\,, \qquad (1)$$

$$H_z' = i\,(\gamma_1 - \frac{\epsilon_y^2}{\gamma_1})\,E_\phi + \frac{m\epsilon_y}{r\gamma_1}\,H_z\,, \qquad (2)$$

and

$$E_\phi'' + U E_\phi' + V E_\phi = 0 , \tag{3}$$

where

$$U = \frac{1}{r}\,(3 - 2\frac{\gamma_1}{\gamma_2}) + \epsilon_x'\,(\frac{1}{\gamma_1} - \frac{1}{\gamma_2}) , \tag{4}$$

$$V = \alpha^2 + \frac{1}{r^2}\,(1 - m^2 - 2\frac{\gamma_1}{\gamma_2} - 2\frac{m\epsilon_y}{\gamma_2}) + \frac{\epsilon_x'}{r}\,(\frac{1}{\gamma_1} - \frac{1}{\gamma_2}) + \frac{m}{r}\,\frac{1}{\gamma_1\gamma_2}\,(\gamma_2\epsilon_y' - \epsilon_x'\epsilon_y) , \tag{5}$$

$$\alpha^2 = (\epsilon_L - n_z^2)\,(\epsilon_R - n_z^2) / (\epsilon_x - n_z^2) , \tag{6}$$

$$\gamma_1 = \epsilon_x - n_z^2 , \tag{7}$$

and

$$\gamma_2 = \gamma_1 - (m^2/r^2) , \tag{8}$$

while ϵ_x, ϵ_y, ϵ_L, and ϵ_R correspond, respectively, to the cold-plasma refractive index components S, D, L and R of Ref. 22.

Equation (3) establishes the boundary conditions at $r \to 0$. For the two cases $m = 0$ and $m \neq 0$, respectively, one obtains

$$E_\phi'' + r^{-1} E_\phi' + (\alpha^2 - r^{-2})\, E_\phi = 0 , \tag{9}$$

and

$$E_\phi'' + 3r^{-1} E_\phi' + [\alpha^2 + (1 - m^2)\, r^{-2}]\, E_\phi = 0 . \tag{10}$$

Since for $r \to 0$, α is slowly varying, (9) and (10) reduce to Bessel equations which together with (1) give

$$\zeta_f(r \to 0) = -ir/2 , \; for \; m = 0 ,$$

$$= -ir\gamma_2/(m\epsilon_y + |m|\gamma_1) , \; for \; m \neq 0 . \tag{11}$$

The plasma surface impedance at $r = r_p$ may now be obtained through numerical integration of (1) and (2). The singularity at $\gamma_1 = 0$ is obviated using the artifice

$\gamma_1 = \epsilon_x - n_z^2 + i\nu n_e(r)/n_e(0)$. The value of $\varsigma_f(r_p)$ approaches a stable limit as $\nu \to 0$. Throughout the computations we assume a weighted Gaussian density profile

$$\frac{n_e(r \le r_o)}{\tilde{n}_e} = \left[1 - (\frac{r}{r_o})^{\chi}\right] \, exp\left[-\frac{1}{2}\,(\frac{r}{r_\sigma})^2\right], \tag{12}$$

where $\tilde{n}_e = n_e(0)$, $n_e(r_0) = 0$, r_σ is the variance of the Gaussian, and χ is the profile weight. Broad profiles occur for large χ while low values of r_σ cause narrow peaked profile shapes. In addition to providing boundary conditions at the origin, (3) spells out the importance of the contributions due to the density gradients in the wave propagation characteristics for the case $m \neq 0$. In a later section we would have the occasion to witness some peculiarities in the antenna loading, presumably due to such effects.

3. THE THREE-DIMENSIONAL LOOP ANTENNA

In this section we enlarge upon the periodic loop-antenna theory of Ref. 21.

3.1 Single element loop antenna

The periodic loop-antenna theory of Ref. 21 is semianalytic in the sense that although the electromagnetic field is determined analytically in terms of the antenna current, the current distribution itself is obtained iteratively. Following the prescription of Ref. 20 we outline a fully analytic determination of the antenna current as well, without recourse to iterative procedures. Equation (30) of Ref. 21 may be cast in the form

$$Z_A I^2(0) + \sum_i \sum_j F_\xi(p_i)\, F_\xi(p_j)\, L(i,j) = 0\,, \tag{13}$$

where the partial impedance matrix element $L(i,j)$ is defined as

$$L(i,j) = \oint [\tilde{E}_\xi(p_i,\xi) - \rho_A\, exp(in_{\xi i}\xi)]\; exp(in_{\xi j}\xi)\; d\xi\,, \tag{14}$$

where ρ_A is the antenna resistance per meter associated with the metallic loss. Extremalizing (13) in the manner of Ref. 20 yields

$$Z_A^{-1} = \sum_i \sum_j L^{-1}(i,j)\,, \tag{15}$$

and

$$F_\xi(p_i) \;=\; I(0)\; Z_A \sum_j L^{-1}(j,i)\;. \tag{16}$$

The integration in (14) involving simple exponentials is readily performed rendering the analysis fully analytic, with the stipulation that the plasma surface impedance matrix ς_P is furnished independently. The fully-analytic, self-consistent boundary value solution of a realistic antenna presented here is significant in the sense that only a few other such examples exist in the antenna literature [23].

3.2 Two element loop antenna

A section of the two element periodic loop antenna is shown in Fig. 1. The upper (U) and the lower (L) loops are inductively coupled and the voltage of each loop may be expressed in the form

$$V_\mu \;=\; Z_{\mu\mu}\; I_\mu(0) \;+\; Z_{\mu\nu}\; I_\nu(0) \tag{17}$$

where each of the subscripts μ and ν ranges over U and L. The analytical procedure of the preceding section is no longer applicable. Instead we follow an iterative scheme starting with an equation paralleling (30) in Ref. 21

$$\begin{aligned}[\; Z_{\mu\mu} \sum_{i\mu} F_{\xi\mu}(p_{i\mu}) \;+\; Z_{\mu\nu} \sum_{i\nu} F_{\xi\nu}(p_{i\nu})\;] \sum_{j\mu} F_{\xi\mu}(p_{j\mu}) \\ +\sum_{i\mu}\sum_{j\mu} F_{\xi\mu}(p_{i\mu})\; L_{\mu\mu}(i,j)\; F_{\xi\mu}(p_{j\mu}) \\ +\sum_{i\nu}\sum_{j\mu} F_{\xi\nu}(p_{i\nu})\; L_{\mu\nu}(i,j)\; F_{\xi\mu}(p_{j\mu}) \;=\; 0\;,\end{aligned} \tag{18}$$

where

$$L_{\mu\nu}(i,j) \;=\; \oint_\mu [\; \tilde{E}_\xi(p_{i\nu},\xi) \;-\; \rho_A\; exp(in_{\xi i}\xi)]\; exp(in_{\xi j}\xi)\; d\xi\;. \tag{19}$$

The stationarity [24] of $Z_{\mu\nu}$ with respect to $F_\xi(p_i)$ together with the constraint $I_U(0) = I_L(0)$ provides the set of simultaneous algebraic equations for the determination of

$F_\xi(p_i)$ in terms of the assumed values of $Z_{\mu\nu}$. The $Z_{\mu\nu}$ are in turn obtained from $F_\xi(p_i)$ using

$$\sum_{i\nu} \sum_{j\mu} F_{\xi\nu}(p_{i\nu})\, F_{\xi\mu}(p_{j\mu})\, [\, Z_{\mu\nu} + L_{\mu\nu}(i,j)\,] = 0. \tag{20}$$

The initial values of $Z_{\mu\nu}$, obtained by assuming the antenna currents existing in the absence of the coupling terms, are given by

$$Z^{-1}_{\mu\nu} = \sum_{i\mu} \sum_{j\nu} L^{-1}_{\mu\nu}(i,j). \tag{21}$$

These results may be extended to any number of coupled antennas in a straightforward manner.

4. THE RESULTS

In this section the computed values of the antenna resistance R, the reactance X, the quality factor Q, and the efficiency η_A are presented. The antenna efficiency is defined as the ratio of the net power delivered into the plasma versus the power entering the antenna terminals. The antenna dissipation accounts for over ninety percent of the total resistive losses in the system, the rest occuring in the wall and the Faraday screen, respectively. The present computations assume that all the sufaces are silvered, but may be readily extrapolated to other surface conditions. ASDEX UPGRADE parameters used as a reference are given in Table I. A fully ionized hydrogen plasma is assumed throughout the computations.

We will regard the position of the singular layer, r_A, as the primary fixed parameter. Such a procedure would enable us to analyze and optimize the antenna performance without the strong masking effect arising from the dominant dependence of the antenna characteristics on r_A. In order to maintain r_A constant, the frequency of operation, f, must be varied as the plasma conditions are varied. The practical implications of such a course will be discussed in Sec. 5.

Once the resonant density n_A, the magnetic field B_0, and $\Lambda/2$, the distance between the adjacent antennas assumed to be in phase opposition are fixed, the frequency, f, is uniquely determined by the resonance condition $\gamma_1(r_A) = 0$. In order to avoid parasitic resonances near the plasma edge, it will be consistently assumed that $n_z \equiv n_{z0} = 2\pi/\Lambda_{z0} = N_A/2r_T$, where N_A is the number of antennas deployed per torus circumference. We will avoid coupling at the higher toroidal harmonics ($n_z = hn_{z0}, h > 1$), which would inevitably introduce secondary resonances between the plasma edge and the principal resonance. The strong coupling to these resonances creates a false impression of improved antenna performance while actually causing surface dissipation accompanied by impurity production.

4.1 Single element antenna

Figure 2 shows the antenna characteristics as a function of the number of the antenna elements deployed over the length of the toroidal circumference. We assume the adjacent antenna elements to be in phase opposition so that $N_A \equiv 2n$. Since the position of the resonance is held fixed, $n_z = ck_z/\omega$ stays constant and ω increases with k_z. As N_A increases, the antenna loading improves sharply due to the increasing ratio of ω/ω_{ci}, reaching a broad maxima near $N_A = 16$, and eventually tapering off due to the field cancellation effects which start to dominate as $\Lambda/2 \rightarrow r_p$. Coupling could, of course, be increased by moving the resonance closer to the plasma edge, but it is not our objective to heat the plasma edge. There is no obvious alternative to using a dense antenna configuration in the longitudinal direction with an adjacent antenna separation of the order of the plasma radius.

Figure 3 confirms the inability of the Alfven waves to penetrate into the plasma core. In quantitative terms efficient coupling may not be feasible for $r_A/r_p \leq 0.67$. Only a marginal improvement in penetration is to be expected from the excitation of the kinetic Alfven wave in a hot plasma because its short absorption distance of a few centimeters [13] would be of little consequence in a plasma of thermonuclear dimensions. There remains the important possibility of a uniform energy deposition via the anamolously enhanced electron thermal conductivity as in the case of the neutral-beam heating, but such considerations are outside the scope of this paper.

The relative insensitivity exhibited by the antenna loading R with respect to large variations in the magnetic field B_0, the maximum plasma density $\tilde{n}_e$, as well as the plasma density at the edge are shown in Figs. 4-6, respectively. Note that in Fig. 4 the changes in the magnetic field are accompanied by proportionate changes in f so that the parameter ω/ω_{ci} having a strong bearing on the antenna loading remains unaffected.

The effect of varying profile shapes on the antenna impedance is to be seen in Figs. 7 and 8. Coupling decreases somewhat for large χ. Variations in r_σ cause even smaller changes in R, except in the region $r_\sigma/r_p \sim 1$ when the gradient effects alluded to in Sec. 2 become conspicuous. Such pathological cases must be avoided.

Figures 9-11 display the predictable effects due to variations in the antenna dimensions. The antenna back is considered to be flush with the wall.

The slow, monotonic deterioration in the loading as the separation between the plasma and the Faraday screen is increased is shown in Fig. 12.

Figure 13 illustrates the scaling of the antenna impedance as a function of the increasing machine size. The parameter labeled SIZE scales the linear dimensions (plasma radius, antenna length etc.) relative to the ASDEX UPGRADE. The magnetic field, the plasma density, the profile shape and the number of antennas (N_A) are held fixed. Apparently, the Alfven wave heating continues to be a viable approach for machines of thermonuclear dimensions under a variety of plasma and magnetic field conditions.

4.2 The two element antenna

Figure 14 depicts the impedance of the upper and the lower antenna elements along with their combined series impedance as a function of N_A. The parameters used for these computations are identical to those of the single element antenna except that $2l$ in Table I now represents the combined length of the two antenna sections. The azimuthal asymmetry introduced by the finite ϵ_y has resulted in unequal loading of the upper and the lower antenna sections. A comparison with Fig. 2 reveals that the coupling for this case is weaker compared to the single element antenna, and the extra complexity is unwarranted.

The effect of changing $2d$, the azimuthal separation between the two elements is depicted in Fig. 15. As expected, the best coupling occurs when the two elements are positioned $\Lambda/2$ apart ($2d = 0.6m$), when the excitation of the $m = \pm 1$ modes is maximum.

5. DISCUSSION

This work is primarily concerned with the optimization of antenna coupling to Alfven waves using an azimuthal three-dimensional loop-antenna. We trust that the findings of this paper are thought-provoking and call for a reconsideration of certain aspects of the experimental practice of the Alfven wave heating.

5.1 Antenna design

An important result with bearing on experimental antenna design concerns the choice of the longitudinal antenna configuration. The existing practice of using $N_A = 4$, as in the case of TCA [11], would result in an antenna loading with $R \sim 20m\Omega$ and $Q \sim 200$. Allowing for a generous improvement in the loading (say by a factor of 3) due to the effects associated with the toroidicity and the plasma current still leaves room for improvement. A precise comparison with the TCA experiment is not possible because the absence of the Faraday shield in the TCA could create substantial parasitic antenna loading with attendent edge heating, impurity production and density increase. Experimentally acceptable coupling does not occur till $N_A \sim 10$.

Thus the remedy consists in using radically larger values of $N_A \sim 16$ from the outset. For the case of the ASDEX UPGRADE this implies using all the available sixteen ports for the purpose of Alfven wave heating. A compromise solution consists in using a dense-cluster-array antenna of a limited longitudinal extent, reminiscent of the grill coupler for the case of the lower-hybrid heating. The truncated antenna obtained in this manner would divert some of the radio-frequency energy to edge heating due to the presence of spectral components with $n_z < n_{z0}$. The extent of this damage is presently being analyzed along with other edge heating effects due to the direct antenna coupling to the torsional Alfven mode, the Faraday shield alignment, the equilibrium plasma current, as well as the toroidicity.

The superior coupling results for $n >> 1$ are in agreement with those of Ref. 14. However, the difference in the antenna models precludes further comparison of our results with those of Ref. 14.

Finally, from Fig. 4 of Ref. 17 one notes that the antenna loading as well as the voltage vary at most by a factor of *three* (compared to a factor of *fifty* in this paper) as n is varied between 2 and 8. However in Ref. 17, one of the resonances is chosen to lie near the plasma edge (see Sec. 4, Ref. 17) so that good coupling persists under all conditions. This is in stark contrast to the present work where we have scrupulously avoided the presence of singularities close to the plasma edge in order to avoid undesirable surface heating effects.

5.2 Impedance tracking

The precise quantitative formulation in this study was made possible by meticulously keeping the position r_A of the resonant layer in the plasma fixed which would otherwise mask the lesser dependence of the antenna impedance on other parameters. In order to maintain r_A constant one is obliged to track the frequency of operation as the plasma parameters vary. Since the most significant changes in R occur from a shift in the position r_A, an obvious tracking method consists in varying f so as to keep R constant, which would then fix r_A, the parameter of primary interest. This purely electronic tracking method dispenses with any dependence upon the less reliable and relatively slow plasma diagnostics and could be performed at an extremely high speed.

The parameter range over which such a tracking method could be applied is limited by the available bandwidth of the source. A much larger tracking range would be possible by the phase control of the dense-cluster-array antenna very much in the manner of the grill coupler. Once again the tracking method consists in maintaining R constant by the proper phasing of the array elements.

5.3 Plasma current and the toroidal effects

The plasma current has the important effect of introducing the discrete Alfven resonances (DAW) [11]. Since this mode occurs at frequencies below the Alfven continuum, we have chosen to avoid this mode through a judicious choice of the operating frequency and antenna parameters as was indicated in the introduction.

Being bulk plasma modes, the DAWs are likely to be susceptible to the toroidal effects, and one is obliged to resort to a toroidal plasma analysis in order to get a quantitative picture. These remarks, however, are not applicable to the case of the CAW heating which, being a local plasma resonance, is affected by toroidicity *primarily* to the extent by which the *effective* n_z is altered. *The role of toroidicity is further reduced by the requirement that in order to obtain acceptable coupling the resonance must be located at* $r_A \geq 0.67 r_p$. For these reasons we are able to leave out both the plasma current and the toroidal effects in this paper.

In Fig. 5 of Ref. 12 one notes that the antenna loading for the toroidal geometry is substantially the same as given by the cylindrical model. The quantitative fraction of the antenna energy coupled to the parasitic azimuthal modes is more difficult to assess. In the pertinent cases of interest one is obliged to limit coupling to the region $r_A \geq 0.67 r_p$ where the toroidal effects are weak and the diversion to the parasitic modes may be within tolerable limits. Thus the toroidicity, while refining the quantitative results presented here, does not detract from our basic findings; namely, that by choosing $n \sim 8$, an improvement in the antenna loading by a factor of *fifty* compared to the $n \sim 2$ case may be realizable.

REFRENCES

[1]. ALFVEN, H., Arkiv. Mat. Astron. Fysik **29B** (1942)2.

[2]. STEPANOV, K. N., Sov. Phys. JETP **34**(1958)892.

[3]. WINTERBERG, F., Ann. of Phys. **25**(1962)174; Z. Naturforsch. **21**(1966)1270.

[4]. GROSSMAN, W., and TATARONIS, J.A., Z. Phys. **261**(1973)217.

[5]. TATARONIS, J. A., and GROSSMAN, W., Nucl. Fus. **16**(1976)667.

[6]. HASEGAWA, A., and CHEN, L., Phys. Rev. Lett. **32**(1974)454.

[7]. CHEN, L., and HASEGAWA, A., Phys Fluids **17** (1974)1399.

[8]. OTT, E., WERSINGER, J.-M., and BONOLI, P. T., Phys Fluids **21**(1978)2306.

[9]. KARNEY, C. F. F., PERKINS, F. W., and SUN, Y.C., Phys. Rev. Lett. **42**(1979)1621.

[10]. STIX, T. H., in Proceedings of the Second Joint Grenoble-Varenna International Symposium on Heating in Toroidal Plasmas, Como, Italy,(1980)631.

[11]. APPERT, K., BALET, B., GRUBER, R., TROYON, F., TSUNEMATSU, T., and VAcLAVIK, J., Ref. 10, (1980)643; in Plasma Physics and Controlled Nuclear Fusion Research, IAEA, Vienna, **II**(1981)43; in Proceedings of the Fourth Topical Conference on Radio-Frequency Plasma Heating, Austin, Texas, (1981)B7.

[12]. APPERT, K., BALET, B., GRUBER, R., TROYON, F., TSUNEMATSU, T., and VAcLAVIK, Nucl. Fusion **22**(1982)903.

[13]. PURI, S., in Plasma and Controlled Nuclear Fusion Research, IAEA, Vienna, **II**(1981)51.

[14]. ROSS, D.W., CHEN, G.L., and MAHAJAN, S. M., Phys. Fluids **25**(1982)652.

[15]. STIX, T. H., and SWANSON. D. G., in Handbook of Plasma Physics (edited by A. A. Galeev and R. N. Sudan, North Holland, New York, 1983).

[16]. BERNSTEIN, I., Phys. Fluids **26**(1983)730.

[17]. HOFMANN, F., APPERT, K., and VILLARD, L., Report LRP 236/84, Ecole Polytechnique Federale de Lausanne, Switzerland (1984).

[18]. ROSS, D. W., YANMING, L., MAHAJAN, S. M., and MICHIE, R. B., Nucl.

Fusion **26**(1986)139.

[19]. RIYOPOULOS, S., and MAHAJAN, S. M., Phys. Fluids **29**(1986)731.

[20]. THEILHABER, K. S., and JACQUINOT, J., Nucl. Fusion **24**(1984)541.

[21]. PURI, S., Phys. Fluids **27**(1984)2156.

[22]. STIX, T. H., in The Theory of Plasma Waves, McGraw-Hill, New York, (1962).

[23]. KING, R.W.P., The Theory of Linear Antennas (Harvard University Press, Cambridge, MA, 1956).

[24]. STORER, J., in Ref. 23, Chap. II, p. 237.

TABLE CAPTION

Table I Reference ASDEX UPGRADE parameters used in the computations.

FIGURE CAPTIONS

Fig. 1 The two-element antenna geometry comprising of pairs of loops with oppositely directed currents. The $m = 0$ field component is almost absent; a small residual contribution stems from the asymmetry in the current distribution due to the finite ϵ_y effect. The wall and the Faraday shield are situated at $x = -c$ and $x = f$, respectively.

Fig. 2 Antenna characteristics as a function of N_A, the number of antenna elements along the longitudinal torus circumference. Note the sharp drop in the antenna loading below $N_A = 10$, where the current experiments like TCA are being conducted. The dot on the abscissa, in this as well as the following figures, corresponds to the reference parameters of Table I.

Fig. 3 Strong dependence of antenna loading on the radial position of the singular layer clearly depicts the difficulty of penetrating the plasma deeper than half its radius. For $r_A/r_p < 0.5$, the large Q values would present formidable coupling problems. The efficiency also drops rapidly.

Fig. 4 The antenna impedance is insensitive to the magnetic field. Note that the frequency of operation increases in proportion to the magnetic field so that ω/ω_{ci} stays constant.

Fig. 5 The antenna loading shows no appreciable decrease even for the high densities associated with the thermonuclear conditions.

Fig. 6 The antenna coupling is unaffected by the edge plasma density.

Fig. 7 The profile weight assumes importance only for the case of extremely flat plasma profiles corresponding to the large values of the profile weight χ.

Fig. 8 For the peaked plasma profiles with a Gaussian width of the order of the plasma radius, the gradient effects could cause an unstable antenna performance. In practical terms, one is to avoid the choice of such plasma profiles.

Fig. 9 The monotonically improving loading with the increase in the antenna length.

Fig. 10 The loading is unchanged due to variations in the antenna width, although there is the obvious improvement in Q.

Fig. 11 The well known result that low values of b would lead to poor coupling.

Fig. 12 The reduction in the loading due to the increasing separation between the plasma and the Faraday screen.

Fig. 13 The SIZE parameter scales the linear dimensions (e.g. the plasma radius, the antenna size) in relation to the ASDEX UPGRADE. This figure shows that the Alfven wave heating continues to be a viable approach for machines of thermonuclear dimensions.

Fig. 14 Substituting the single-element antenna with a two-element antenna of equal total length causes impairment in the loading and the extra complexity is not warranted.

Fig. 15 The effect of changing $2d$, the azimuthal separation between the two antenna elements. As expected, the best coupling occurs when the two elements are positioned $\Lambda/2$ apart ($2d = 0.6m$), when the excitation of the $m = \pm 1$ mode is maximum.

B_0	magnetic field (T)	3.75
$\tilde{n}_e$	peak density (m^{-3})	1.5×10^{19}
$n_e(r_p)$	edge density (m^{-3})	1.5×10^{17}
X	profile weight	2
r_T	toroidal radius (m)	1.65
r_p	poloidal radius (m)	0.5
r_σ / r_p	normalized variance	4
N_A	antenna elements	16
$2l$	antenna length (m)	0.8
$2w$	antenna width (m)	0.15
$2b$	antenna breadth (m)	0.15
r_A / r_p	normalized position of the resonance	0.67

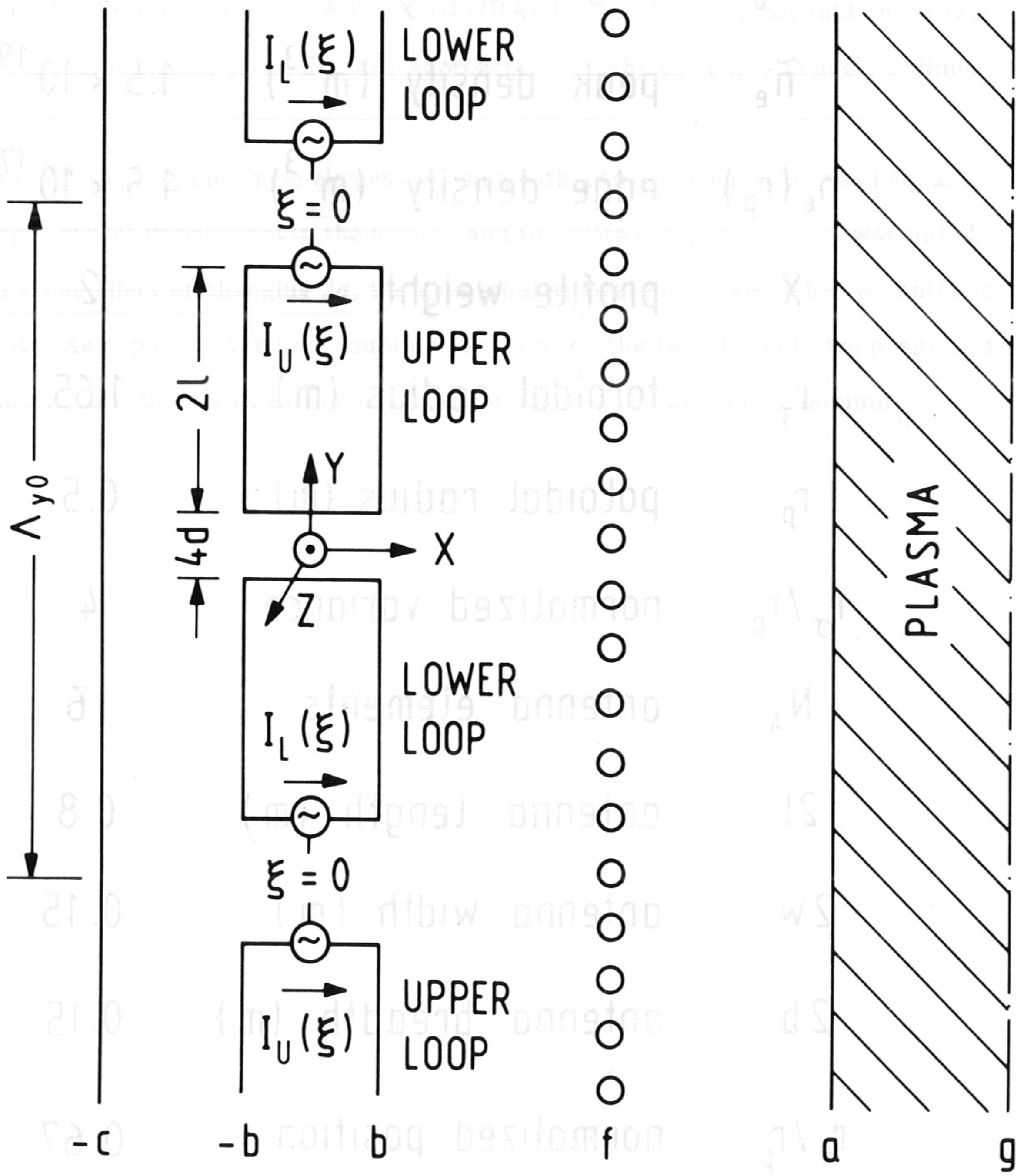

LOWER LOOP
UPPER LOOP
LOWER LOOP
UPPER LOOP
$I_L(\xi)$
$I_U(\xi)$
$I_L(\xi)$
$I_U(\xi)$
$\xi = 0$
$\xi = 0$
Λ_{y0}
$2l$
$4d$
X
Y
Z
PLASMA
-c
-b
b
f
a
g

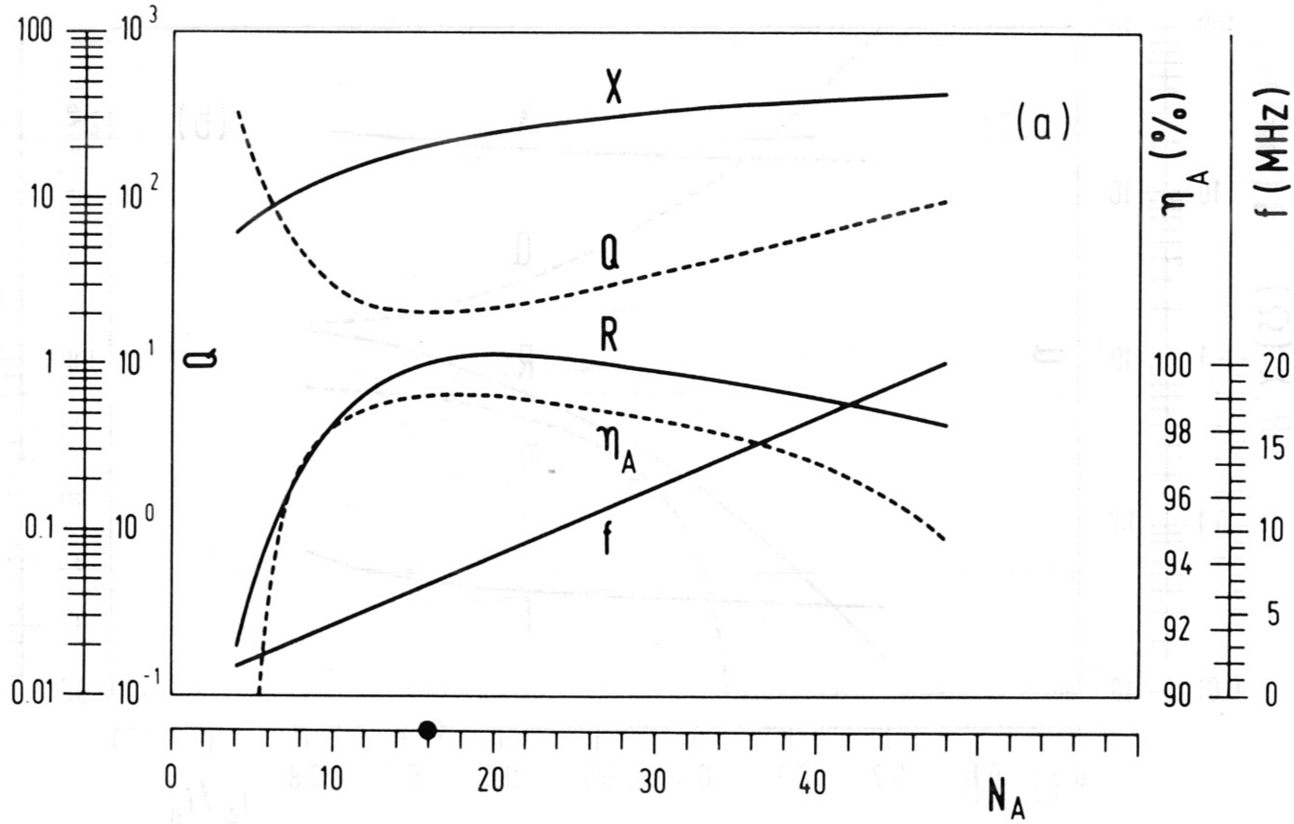

(a)
X
Q
R
η_A
f
R, X (Ω)
Q
η_A (%)
f (MHz)
N_A
100
10
1
0.1
0.01
10^3
10^2
10^1
10^0
10^{-1}
100
98
96
94
92
90
20
15
10
5
0
0
10
20
30
40

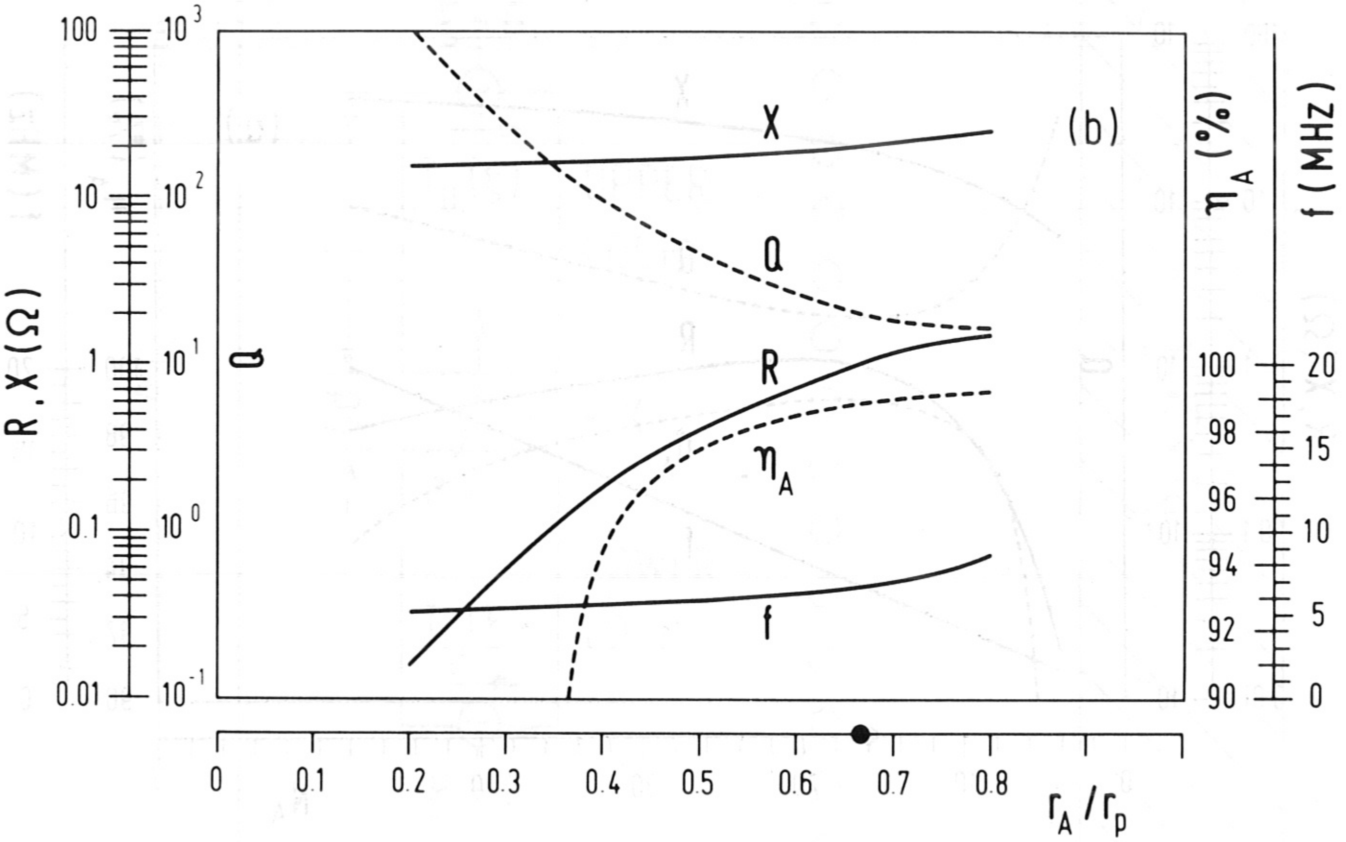

R, X (Ω)
Q
100
10
1
0.1
0.01
10^3
10^2
10^1
10^0
10^-1
X
Q
R
η_A
f
(b)
η_A (%)
f (MHz)
100
98
96
94
92
90
20
15
10
5
0
0
0.1
0.2
0.3
0.4
0.5
0.6
0.7
0.8
r_A / r_p

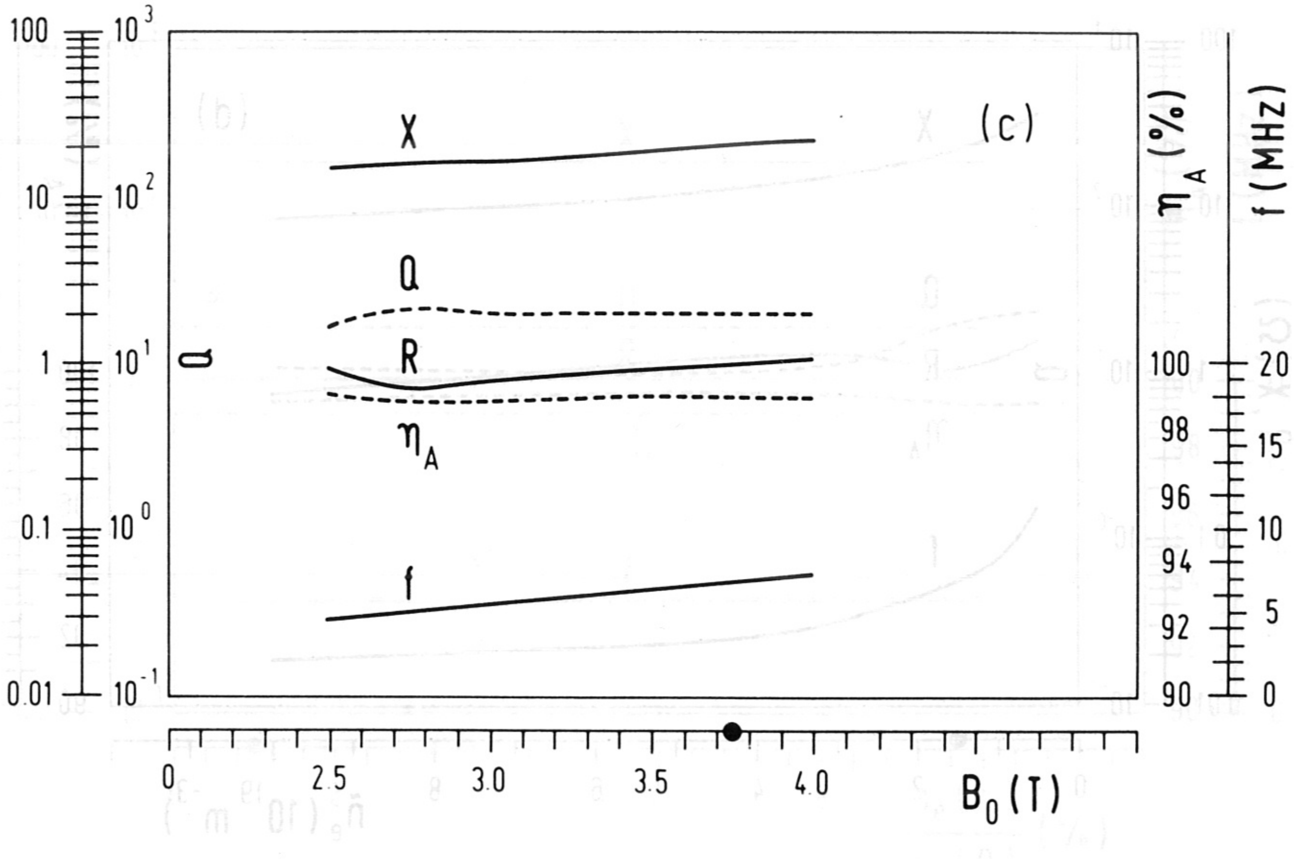
(c)
X
Q
R
η_A
f
R, X (Ω)
100
10
1
0.1
0.01
10^3
10^2
10^1
10^0
10^{-1}
Q
η_A (%)
100
98
96
94
92
90
f (MHz)
20
15
10
5
0
0
2.5
3.0
3.5
4.0
B_0 (T)

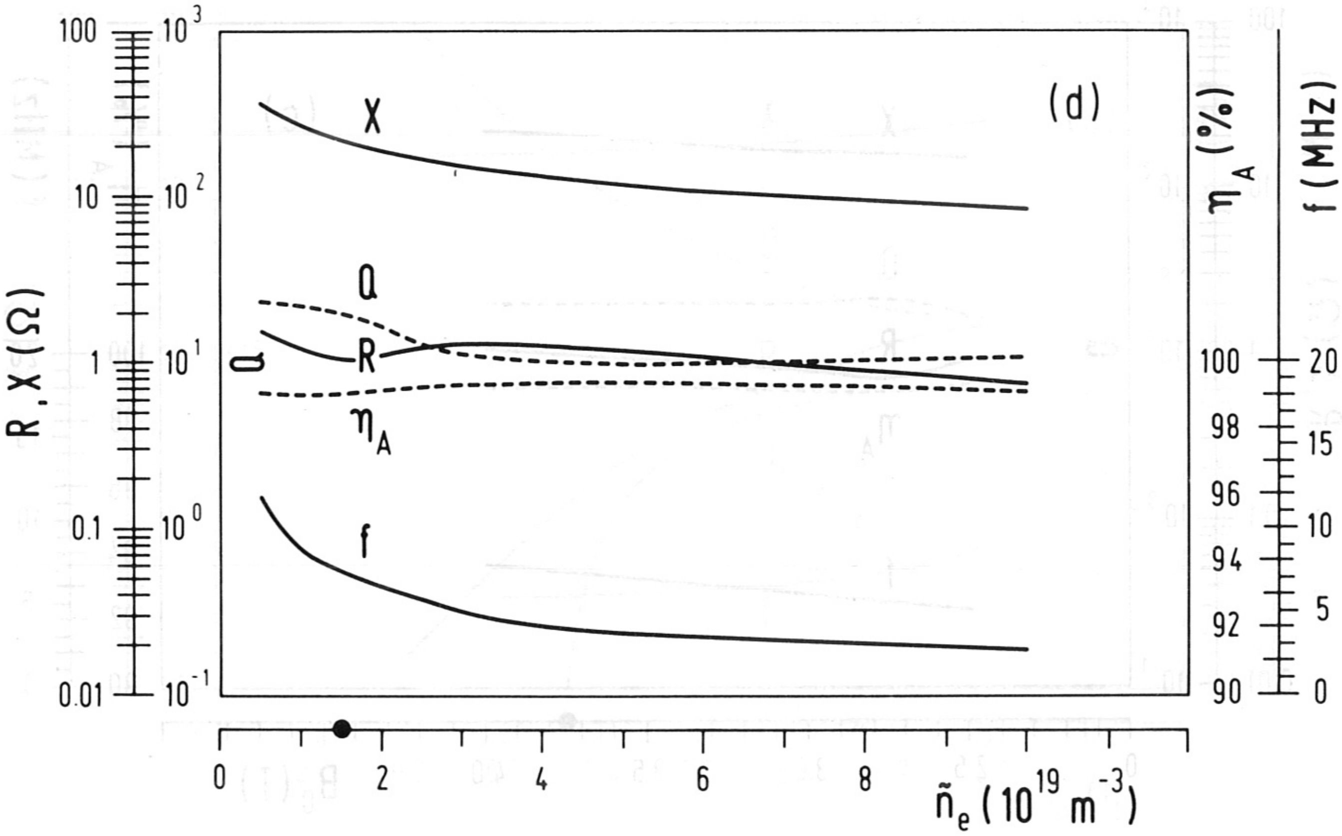

R , X (Ω)
100
10
1
0.1
0.01
10^3
10^2
10^1
10^0
10^{-1}
(d)
X
Q
R
η_A
f
η_A (%)
f (MHz)
100
98
96
94
92
90
20
15
10
5
0
0
2
4
6
8
$\tilde{n}_e$ (10^{19} m^{-3})

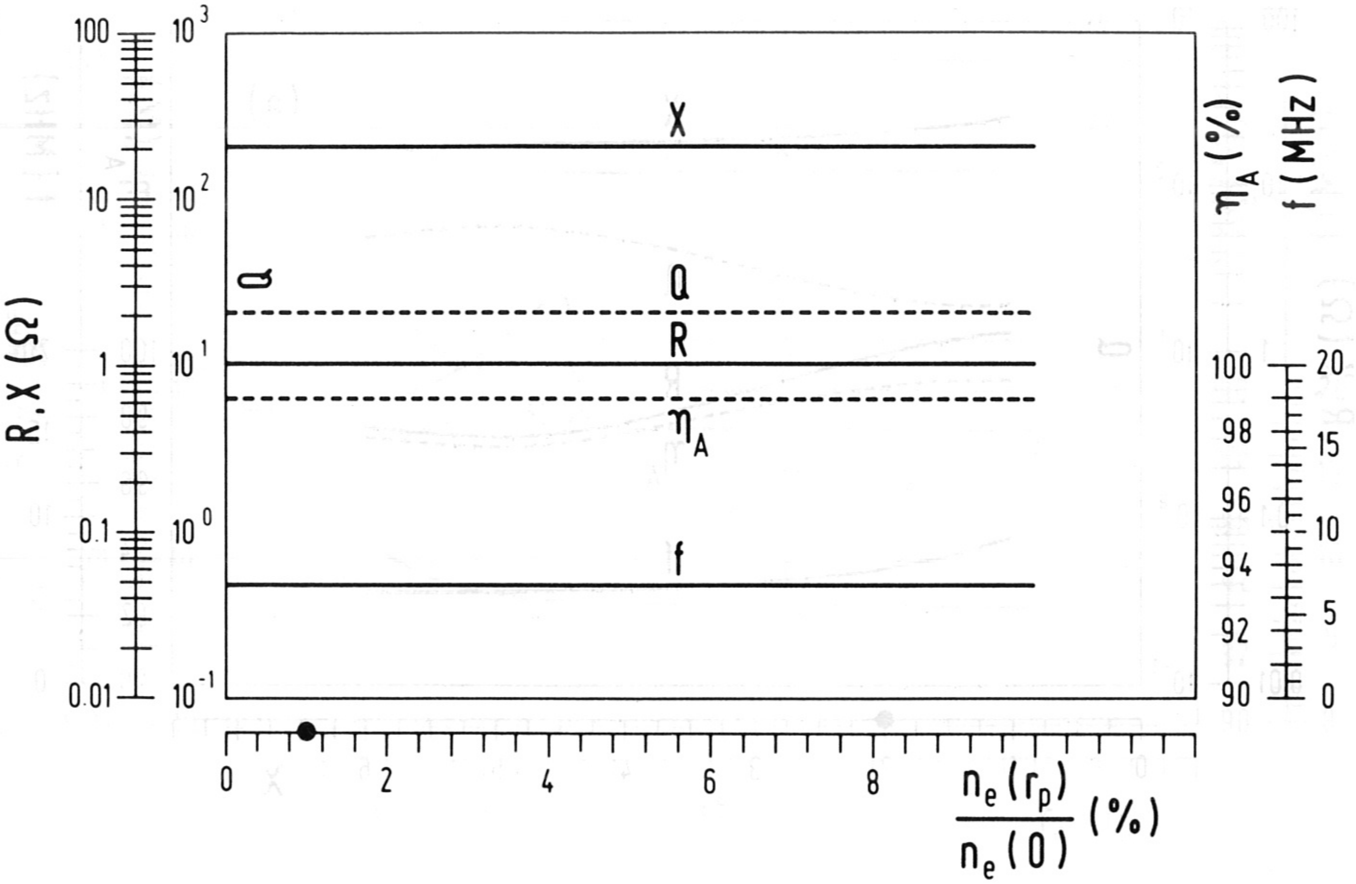

R, X (Ω)
100
10
1
0.1
0.01
10^3
10^2
10^1
10^0
10^{-1}
Q
X
Q
R
η_A
f
η_A (%)
f (MHz)
100
98
96
94
92
90
20
15
10
5
0
0
2
4
6
8
$\frac{n_e(r_p)}{n_e(0)}$ (%)

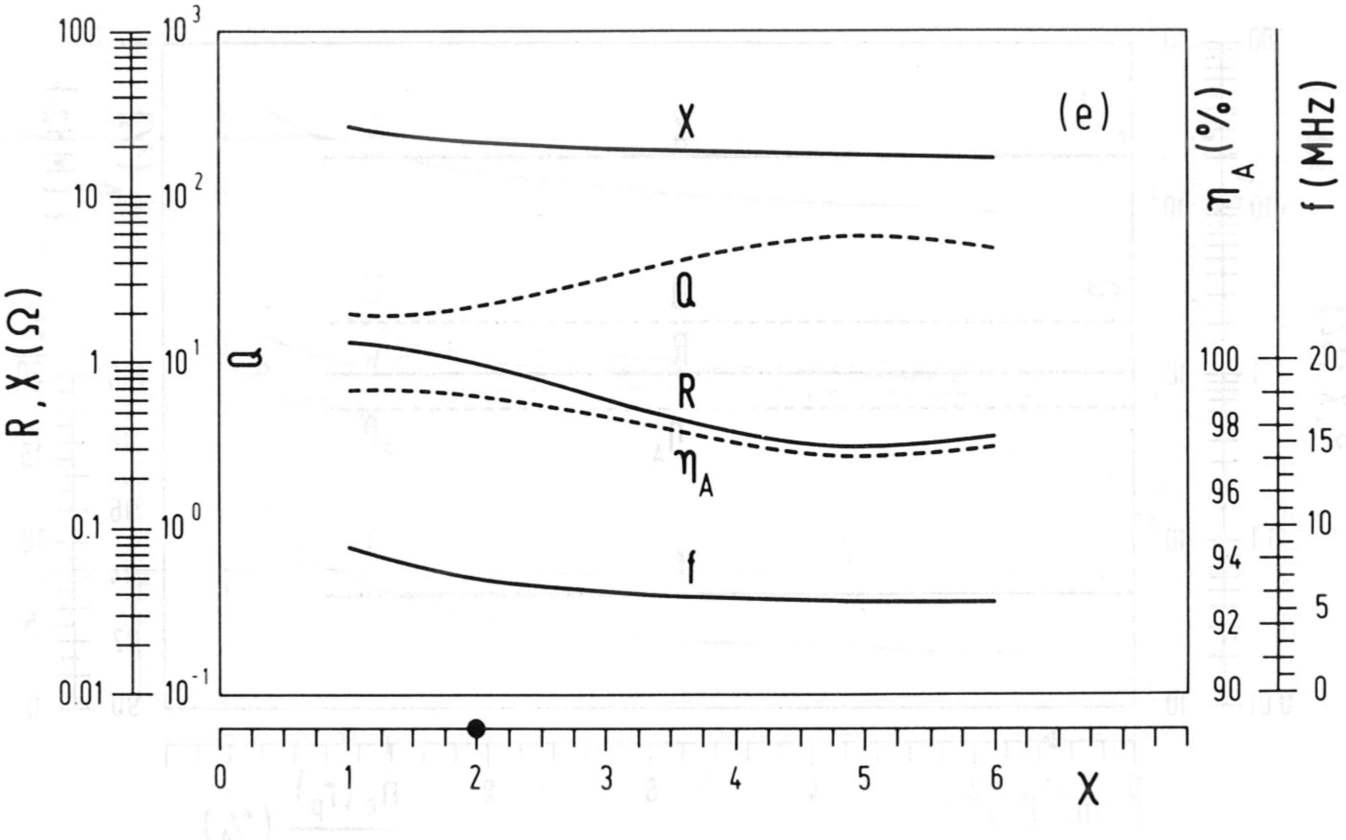
R, X (Ω)
100
10
1
0.1
0.01
10^{3}
10^{2}
10^{1}
10^{0}
10^{-1}
Q
(e)
X
Q
R
η_A
f
η_A (%)
f (MHz)
100
98
96
94
92
90
20
15
10
5
0
0
1
2
3
4
5
6
X

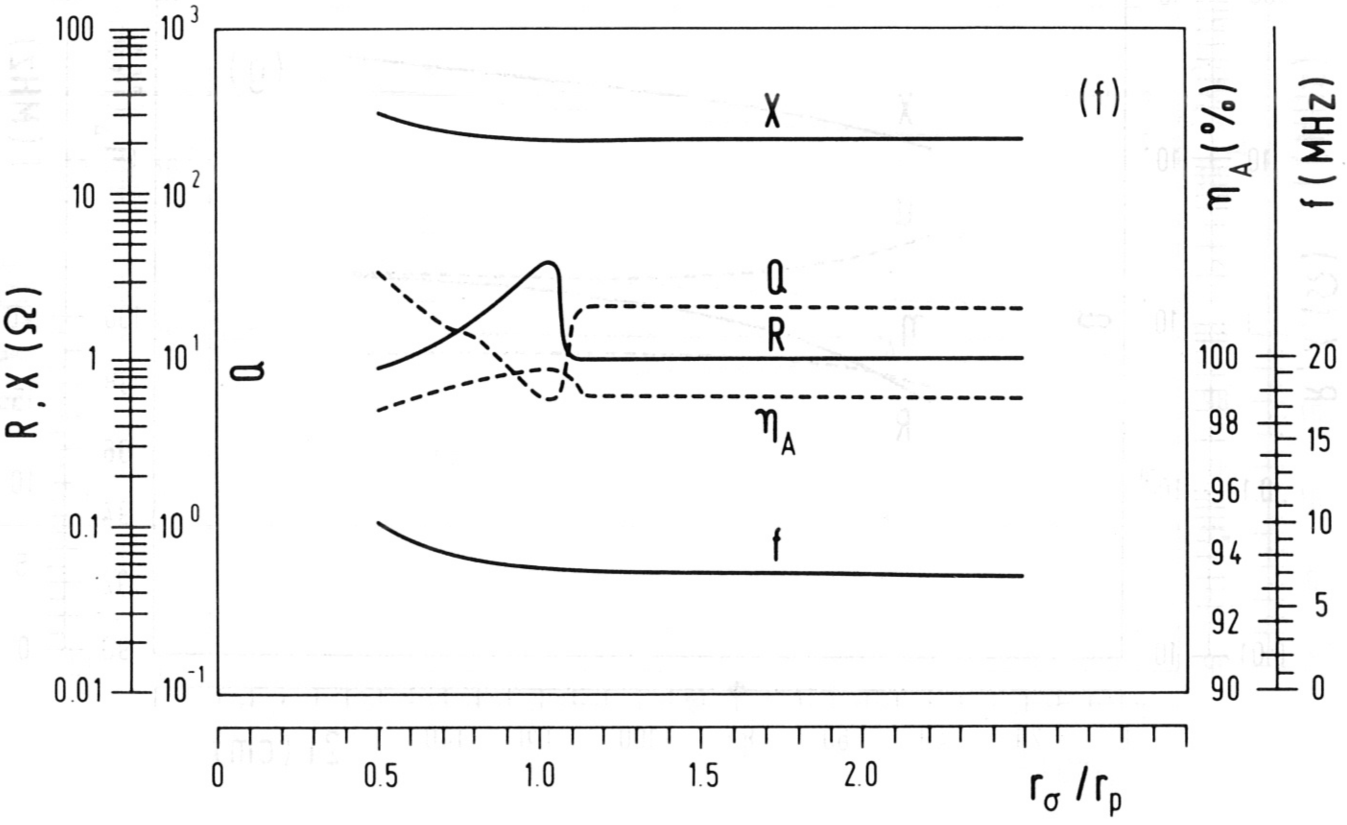

R , X (Ω)
Q
η_A (%)
f (MHz)
(f)
X
Q
R
η_A
f
100
10
1
0.1
0.01
10^3
10^2
10^1
10^0
10^-1
100
98
96
94
92
90
20
15
10
5
0
0
0.5
1.0
1.5
2.0
r_σ / r_p

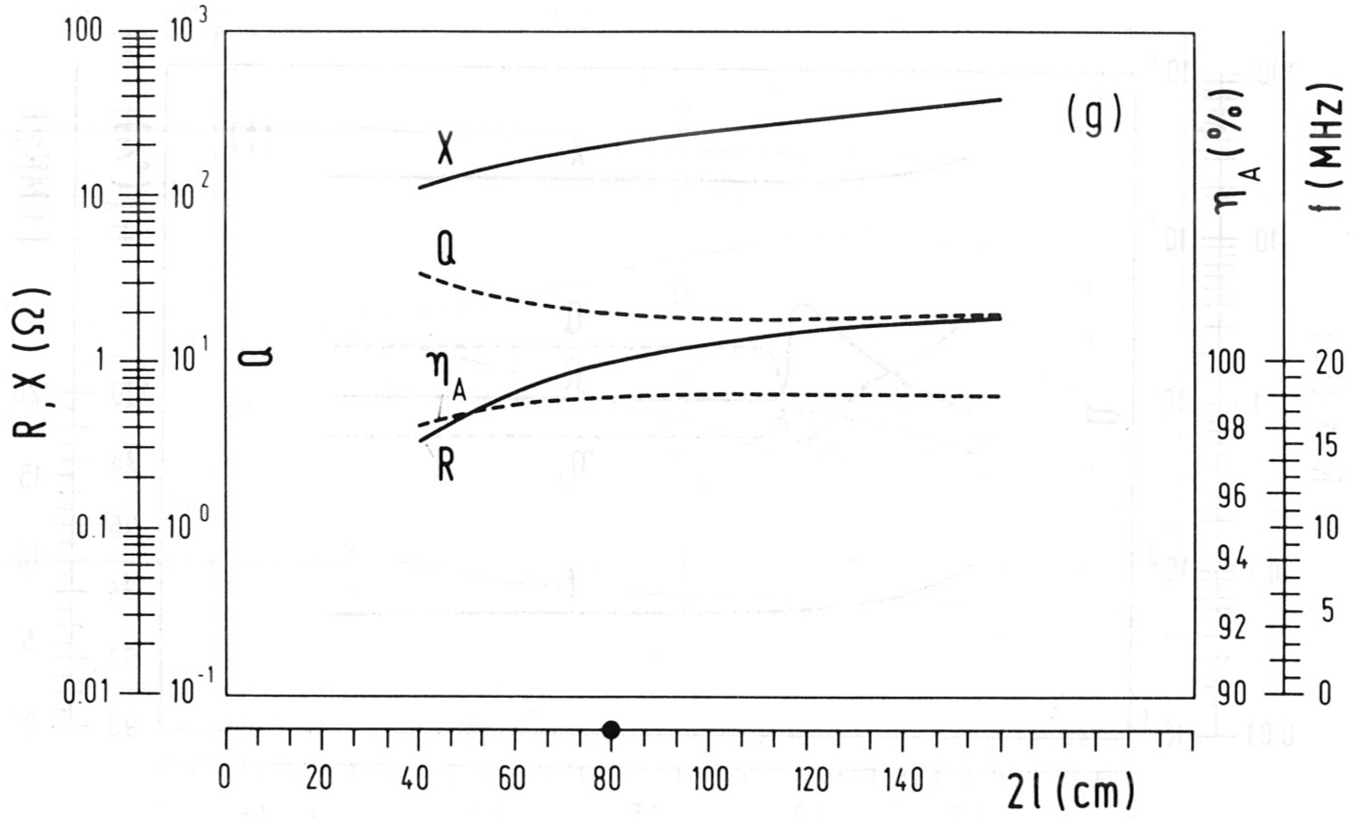

R, X (Ω)
Q
100
10
1
0.1
0.01
10^3
10^2
10^1
10^0
10^{-1}
X
Q
η_A
R
(g)
η_A (%)
f (MHz)
100
98
96
94
92
90
20
15
10
5
0
0
20
40
60
80
100
120
140
2l (cm)

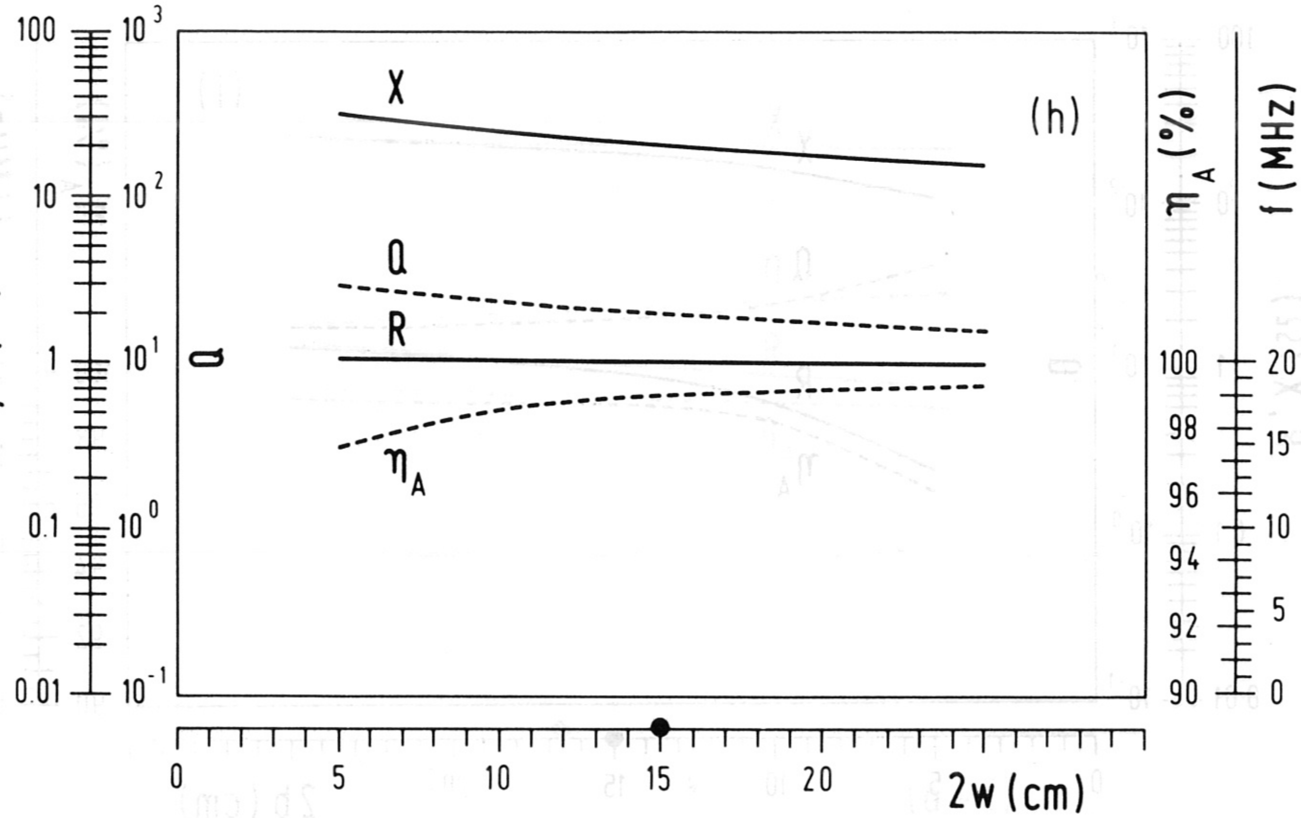

R, X (Ω)
100
10
1
0.1
0.01
10^3
10^2
10^1
10^0
10^{-1}
Q
X
Q
R
η_A
(h)
η_A (%)
100
98
96
94
92
90
f (MHz)
20
15
10
5
0
0
5
10
15
20
2w (cm)

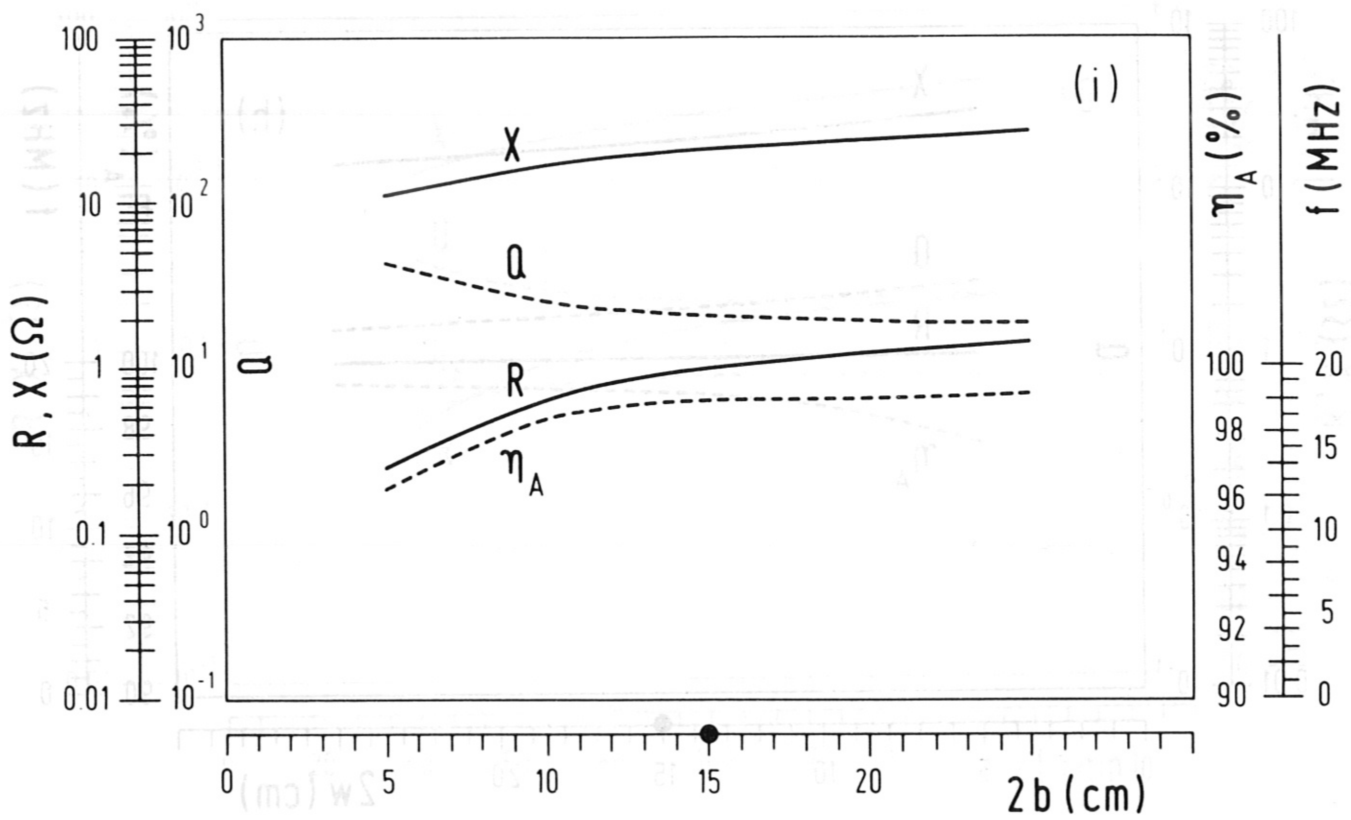

(i)
X
Q
R
η_A
R, X (Ω)
100
10
1
0.1
0.01
10^3
10^2
10^1
10^0
10^{-1}
Q
η_A (%)
100
98
96
94
92
90
f (MHz)
20
15
10
5
0
0
5
10
15
20
2b (cm)

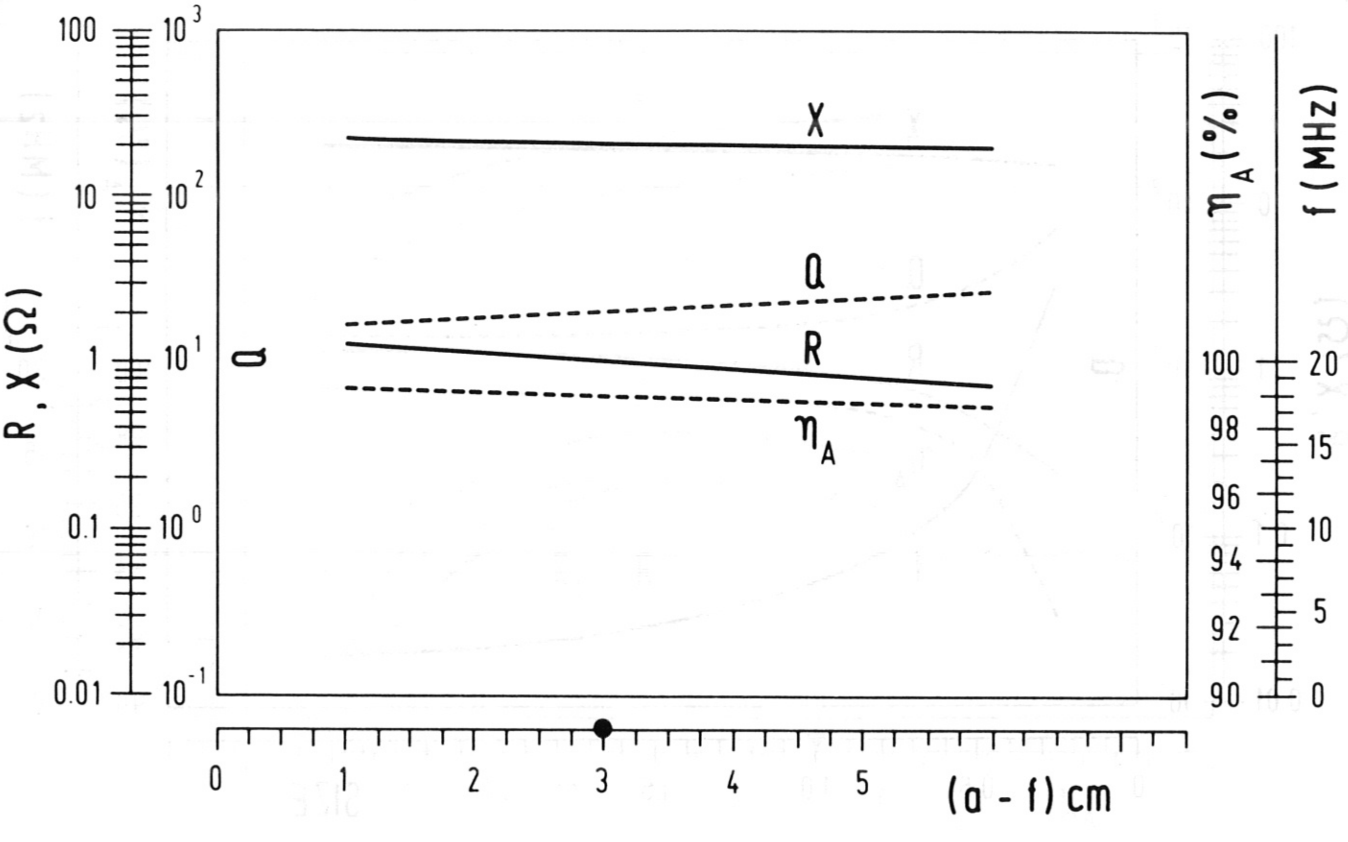

100
10
1
0.1
0.01
R , X (Ω)
10^3
10^2
10^1
10^0
10^-1
Q
X
Q
R
η_A
η_A (%)
100
98
96
94
92
90
f (MHz)
20
15
10
5
0
0
1
2
3
4
5
(a - f) cm

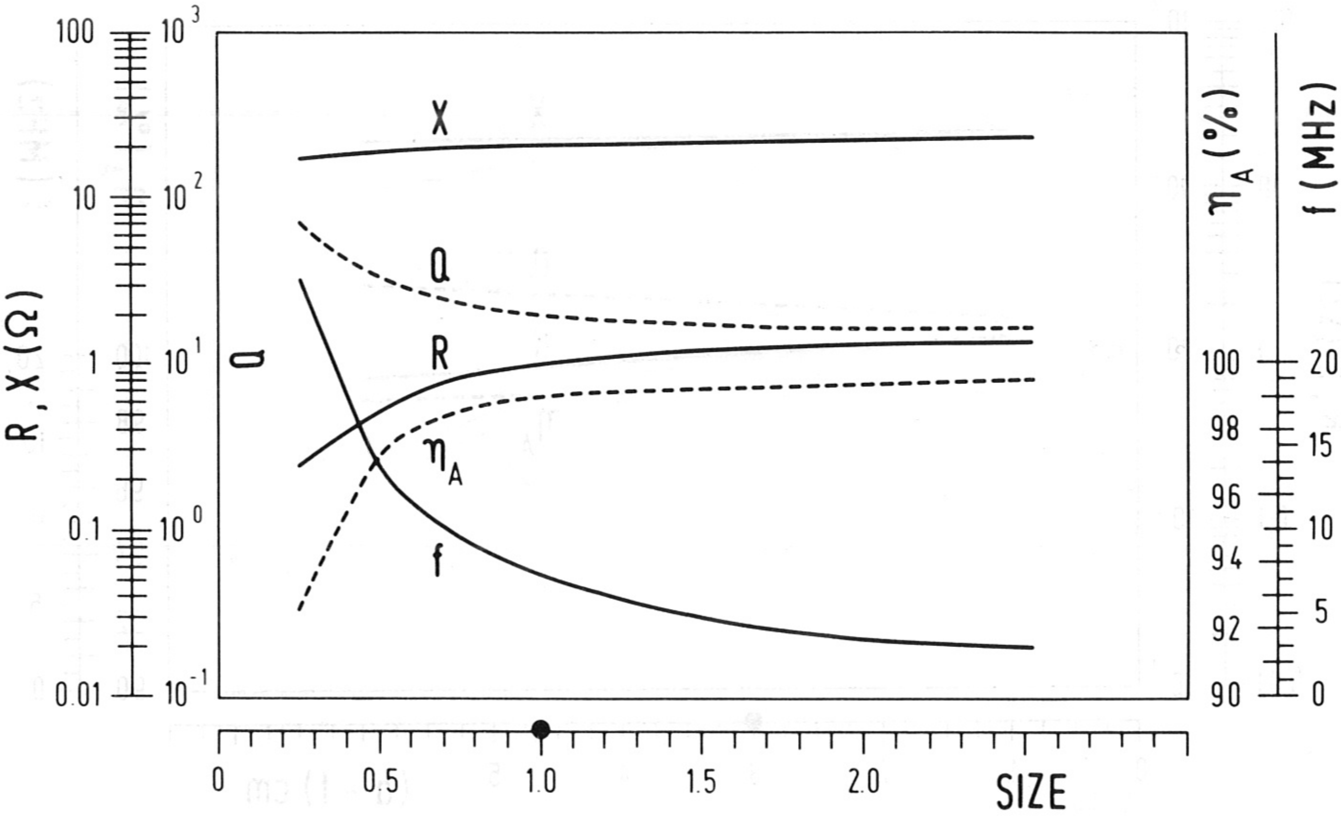

R, X (Ω)
Q
η_A (%)
f (MHz)
X
Q
R
η_A
f
100
10
1
0.1
0.01
10^3
10^2
10^1
10^0
10^{-1}
100
98
96
94
92
90
20
15
10
5
0
0
0.5
1.0
1.5
2.0
SIZE

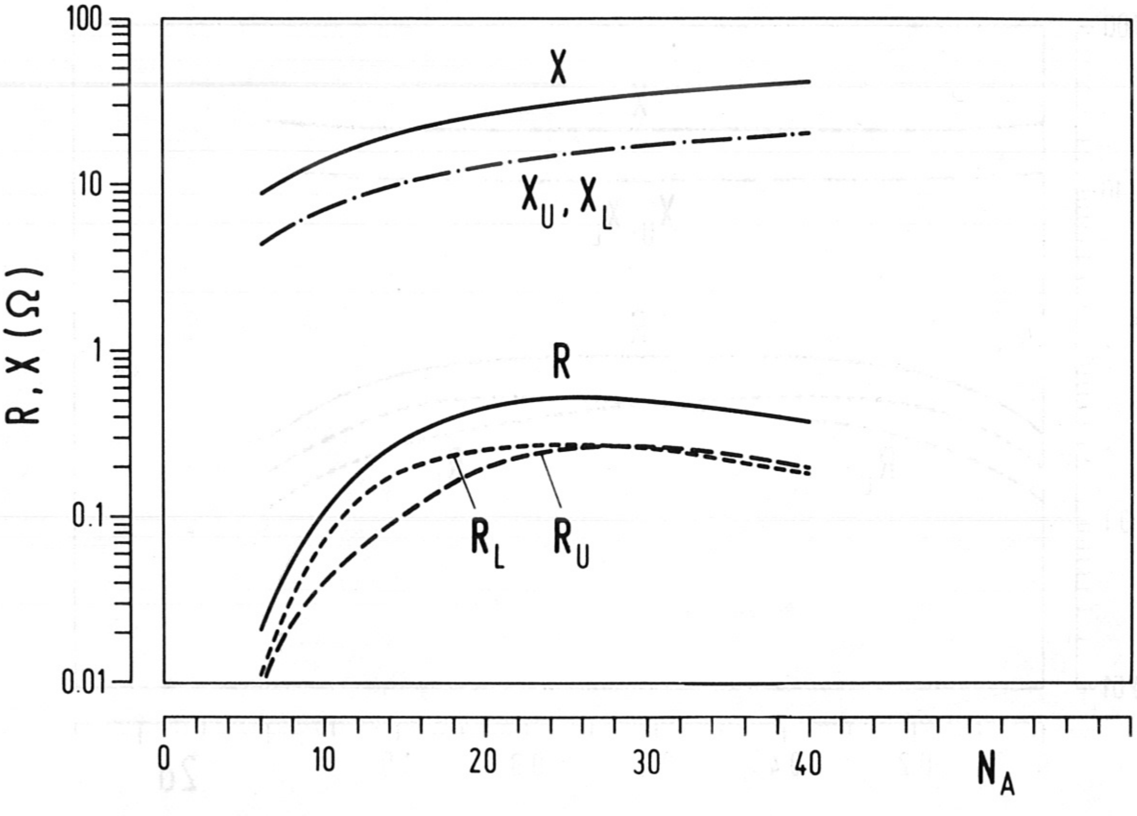

100
10
1
0.1
0.01
R, X (Ω)
X
X_U, X_L
R
R_L
R_U
0
10
20
30
40
N_A

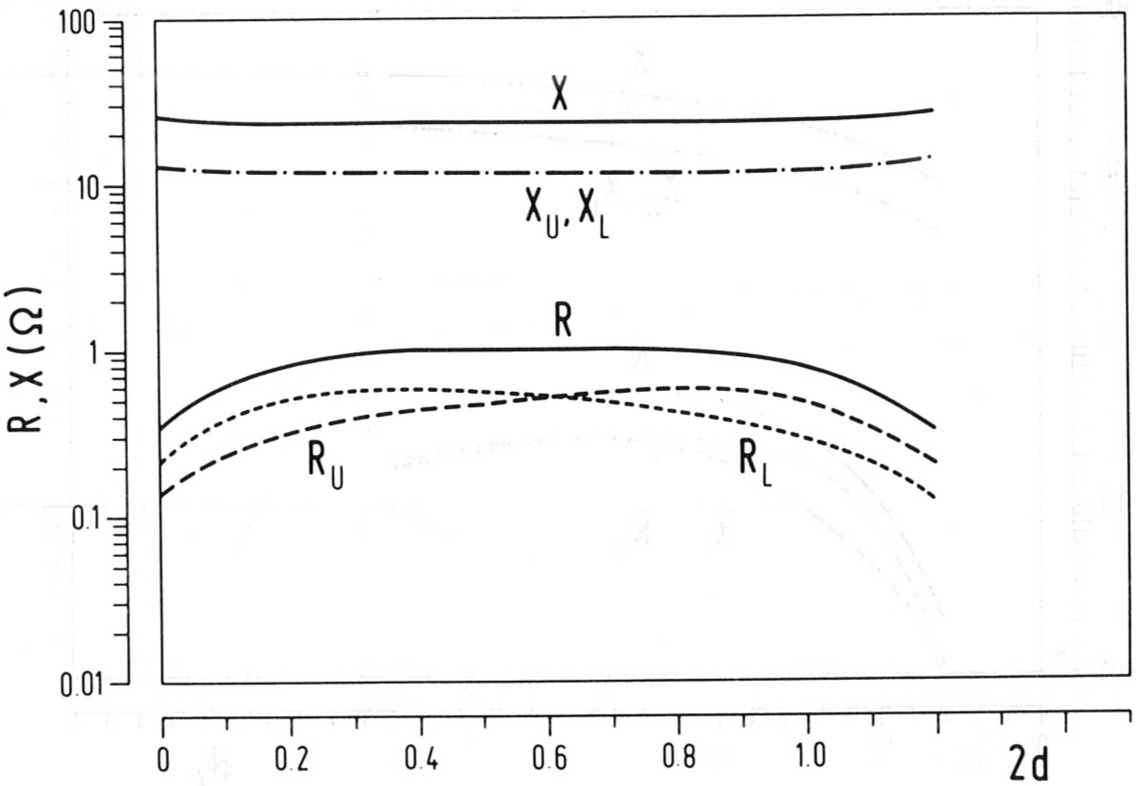

100
10
1
0.1
0.01
R, X (Ω)
X
X_U, X_L
R
R_U
R_L
0
0.2
0.4
0.6
0.8
1.0
2d